ACOUSTICAL BEHAVIOUR OF CONICAL MUFFLER WITH SINGLE-INLET AND SINGLE-OUTLET: A 3-D SEMI-ANALYTICAL APPROACH

Akhilesh Mimani

School of Mechanical Engineering
The University of Adelaide, Adelaide SA 5005, Australia
Email: akhilesh.mimani@adelaide.edu.au

Abstract

This paper analyses the acoustical attenuation behaviour of a conical chamber muffler having a Single-Inlet and Single-Outlet (SISO) by means of a 3-D semi-analytical formulation based on modal expansion of the acoustic field and the Green's function approach. The 3-D acoustic field inside the rigid-wall conical chamber is expressed in terms of the spherical Bessel and Neumann functions of non-integer order, the Legendre and associated Legendre functions of integer order and non-integer degree and the circular functions. The conical chamber muffler is characterised using the uniform piston-driven model in terms of the impedance [$\mathbf{Z}$] matrix parameters (equivalently, the acoustic pressure response function) obtained by computing the average of the 3-D Green's function over the surface area of the inlet/outlet ports modelled as rigid pistons. The 3-D semi-analytical approach enables one to taken into account, effect of relative azimuthal angular location between the inlet and outlet ports on the TL performance by consideration of the non-axisymmetric or azimuthal transverse modes (in addition to the symmetric transverse modes) in the modal summation of the acoustic field. The Transmission Loss (TL) graphs computed by using the 3-D semi-analytical formulation are found to be in an excellent agreement with that obtained from the 3-D FEA, thereby validating the technique presented in this work. Design guidelines for obtaining a broadband TL performance are suggested in terms of optimal (polar and azimuthal) angular and radial location of the ports on the appropriate pressure nodes which is a practically useful outcome of this investigation.

1. Introduction

Variable area ducts of conical geometry are used in different engineering applications such as air-conditioning and gas-distribution systems, intake and exhaust ductwork of compressors, breathing system of internal combustion engines, fans and in electro-pneumatic transducers. The 1-D wave propagation in variable area ducts is a subject matter of several investigations [1-8]. Rayleigh [1] was the first to investigate the acoustic wave propagation in conical ducts wherein it was shown that the amplitude of sound varies inversely as the solid angle of the cone, and that the intensity varies directly as the square of the same angle. Webster [2] obtained closed-form solutions for the acoustic field inside conical, exponential, Bessel and Gaussian horns based on 1-D plane wave analysis. Mawardi [3] obtained different relations for the axial variation of cross-sectional radius of a variable area duct for which, a closed-form analytical solution may be obtained for 1-D wave propagation. Davies and Doak [4] analysed conical ducts carrying uniform mean flow based on 1-D spherical wave propagation. Miles [5] obtained the Transfer [$\mathbf{T}$] matrix for a variable area duct (nozzle) carrying compressible subsonic mean flow. It is noted that the formal solution of the 1-D spherical wave equation is obtained in terms of the zero-order spherical Bessel function and indeed, it is identical with the solution of the Webster's horn equation for a conical duct that is based on 1-D axial plane wave propagation [6]. Easwaran and Munjal [7] obtained the analytical solution of the acoustic pressure field and consequently, the [$\mathbf{T}$] matrix inside a conical and exponential shaped muffler based on 1-D axial plane

approach wherein the effects of incompressible mean flow was considered. It is noted that the sudden-area discontinuity associated with a port (as in a simple expansion chamber) were not considered, rather the attenuation characteristics of an isolated conical and exponential duct was considered. Gupta *et al.* [8] presented an improved stepped duct segmentation approach for analysing plane wave propagation in non-uniform ducts carrying subsonic mean flow.

Multi-dimensional wave propagation in variable area (non-uniform) ducts using numerical as well as analytical techniques has also received considerable interest [9-14]. Astley and Eversman analysed multi-modal wave propagation in non-uniform ducts with mean flow using the weighted residual method [9] and FEA [10]. A pioneering work in the analytical study of multi-dimensional wave propagation in gradually varying area ducts was due to Alfredson [11] wherein the entire duct was notionally divided into a number of stepped duct segments (of uniform cross-section area) where the radius of the adjacent segments are so taken that they closely mimic the profile of the variable area duct. However, it is noted that only axisymmetric (radial) and axial modes were included whilst the azimuthal or circumferential modes was not considered. The analytical solution of the acoustic field in the duct was in a good agreement with experimental values for an exponential duct, thereby validating his analytical approach. Different analytical/numerical techniques for modelling wave propagation inside a wine bottle (an example of a gradually varying flare) were reviewed by Cummings [12]. Willatzen [13] analysed the axisymmetric 3-D wave propagation in a rigid-wall conical duct carrying a mean flow by means of an analytical Green's function based on the modal expansion of the acoustic field expressed in terms of Legendre functions of non-integer degree and the spherical Hankel functions. It is noted that since the non-axisymmetric or azimuthal modes were not considered, the associated Legendre and circular functions do not feature in the analytical solution of the acoustic field. Denia *et al.* [14] presented a similar 3-D analytical approach to evaluate the acoustic attenuation performance of mufflers with conical inlet and outlet ducts of cross-sectional area equal to that of circular cylindrical middle chamber at the duct-chamber interface. It is noted that due to the concentric location of the inlet/outlet conical ducts and co-axial orientation of the conical flare (with respect to the middle cylindrical chamber), it was not necessary to consider non-axisymmetric modes in the modal solution. Furthermore, the muffler configuration analysed did not have sudden-area discontinuities that are typically used in circular/elliptical cylindrical expansion chamber with end/side ports.

The aforementioned papers either analyse acoustic wave propagation in a variable area duct based on the simple 1-D plane/spherical wave model or whilst considering multi-dimensional wave propagation, include only the axisymmetric modes in the modal expansion. However, the problem of analysing the acoustic attenuation behaviour of a variable area duct having inlet/outlet ports by considering the complete 3-D acoustic field that includes both axisymmetric and non-axisymmetric or circumferential modes is not investigated yet. The objective of this paper is therefore, to analyse the Transmission Loss (TL) performance of a conical muffler having a Single-Inlet and Single-Outlet (SISO) based on a 3-D semi-analytical modal summation approach that includes both axisymmetric and non-axisymmetric modes, thereby enabling one to take into account, arbitrary location of inlet/outlet ports. The motivation for considering a conical geometry is because of its use in several engineering applications (indicated before) and also to analyse the combined effect of sudden-area expansion (at port-chamber interface) and gradually varying cross-section, i.e., the flare of the conical chamber on the TL characteristics.

This paper is organised as follows. Section 2 presents the theoretical formulation for characterising a 2-port rigid-wall conical muffler with arbitrary port location either on the spherical end faces or side surface using a 3-D semi-analytical approach based on the complete modal expansion (including the azimuthal modes) and the Green's function method. Section 3 presents the TL graphs for different SISO conical muffler configurations obtained using the 3-D semi-analytical approach, compares the results with 3-D FEA prediction and analyses the effect of port location. The paper is concluded in Section 4 wherein configurations exhibiting a broadband TL performance are mentioned.

2. Theoretical Formulation

2.1 Characterisation of a single-inlet and single-outlet (SISO) muffler

A 2-port muffler, i.e., a SISO system is characterised using an impedance [**Z**] matrix formulation shown hereunder [15].

$$\left\{ \begin{matrix} p_1 \\ p_2 \end{matrix} \right\} = [\mathbf{Z}] \left\{ \begin{matrix} v_1 \\ v_2 \end{matrix} \right\}, \quad [\mathbf{Z}] = \begin{bmatrix} Z_{11} & Z_{12} \\ Z_{21} & Z_{22} \end{bmatrix}_{2 \times 2}, \tag{1, 2}$$

where p_1 and p_2 are the acoustic pressure (Pa) whilst v_1 and v_2 are the acoustic mass velocities $(\mathrm{kg \cdot s^{-1}})$ at the ports 1 and 2, respectively. It is noted that the direction of acoustic mass velocities is considered positive *looking into* the muffler and a harmonic time-dependence is assumed so that $p_i = p_i e^{j\omega t}$ and $v_i = v_i e^{j\omega t}$, $i = 1, 2$. Furthermore, $j = \sqrt{-1}$, t denotes time (in seconds), ω is excitation angular frequency $(\mathrm{radian \cdot s^{-1}})$ given by $2\pi f$, where f is the frequency in Hz. In the ensuing subsection, a SISO conical muffler is characterised using the uniform piston-driven model via the 3-D Green's function approach in terms of the $[\mathbf{Z}]$ matrix parameters. It is noted that walls of the conical chamber are considered rigid (with no absorptive linings), therefore, a conservative system is considered. Furthermore, a zero mean flow is assumed implying that the system satisfies acoustic reciprocity [16].

2.2 Acoustic pressure field in a rigid-wall conical chamber: Solution of the 3-D homogeneous Helmholtz equation

The acoustic wave propagation in a conical chamber (of circular cross-section) is analysed by first considering the 3-D homogeneous Helmholtz equation in spherical polar co-ordinates given by [17]

$$\left(\nabla^2 + k_0^2 \right) p = 0, \quad \nabla^2 = \frac{1}{r^2} \left\{ \frac{\partial}{\partial r} \left(r^2 \frac{\partial}{\partial r} \right) + \frac{1}{\sin \theta} \frac{\partial}{\partial \theta} \left(\sin(\theta) \frac{\partial}{\partial \theta} \right) + \frac{1}{\sin^2 \theta} \frac{\partial^2}{\partial \phi^2} \right\}, \tag{3, 4}$$

where r is the radial co-ordinate measured from the hypothetical apex $\mathbf{O}$ of the conical chamber shown in Fig. 1(a), θ and ϕ are the polar and azimuthal angular co-ordinates, respectively, $k_0 = \omega/c_0$ is the excitation wavenumber and c_0 denotes the sound speed. The separation of acoustic pressure field $p(r, \theta, \phi) = R(r)\Theta(\theta)\Phi(\phi)$ yields the following ordinary differential equations

$$\frac{d^2 \Phi}{d\phi^2} + \mu^2 \Phi = 0, \quad \frac{1}{\sin \theta} \frac{d}{d\theta} \left(\sin \theta \frac{\partial \Theta}{\partial \theta} \right) + \left(\eta^2 - \frac{\mu^2}{\sin^2 \theta} \right) \Theta = 0 \text{ and } \frac{d}{dr} \left(r^2 \frac{dR}{dr} \right) + \left(k_0^2 r^2 - \eta^2 \right) R = 0, \tag{5-7}$$

governing wave propagation along the azimuthal, polar angular and radial directions, respectively. In Eqs. (5-7), μ and η are separation constants where $\eta^2 = \nu(\nu + 1)$. It is noted that the domain given by $[r = r_{\mathrm{inner}}, r_{\mathrm{outer}}] \times [\theta = 0, \theta_0] \times [\phi = 0, 2\pi]$ spans the rigid-wall conical chamber where r_{inner} and r_{outer} connotes the inner and outer radius of the spherical end surface, respectively, whilst θ_0 denotes the half-opening angle (flare) of the conical chamber. The acoustic pressure field satisfies the periodicity condition $p(\phi) = p(\phi + 2\pi)$ along the azimuthal direction (due to continuity requirement) which implies that $\mu = m = 0, 1, 2, \ldots \infty$, i.e., an integer. Unlike the solution of spherical wave equation for spherical [18] or hemispherical cavity [19], the constant ν in Eq. (7) for a conical chamber cannot be taken as an integer, i.e., $\nu \neq 0, 1, \ldots$, rather, it is a positive real number determined by the solution of

$$u_\theta = \left(\frac{j}{k_0 \rho_0 c_0} \right) \frac{1}{r} \frac{\partial p}{\partial \theta} \bigg|_{\theta = \theta_0} = 0 \implies \frac{\partial \Theta(\theta)}{\partial \theta} \bigg|_{\theta = \theta_0} = 0, \tag{8}$$

because the conical chamber must satisfy the rigid-wall boundary condition along the polar angular direction at the flare angle $\theta = \theta_0$. (Here, u_θ is the acoustic velocity component along the polar angular direction and ρ_0 is the ambient density.) To this end, Eq. (6) is transformed (after considerable algebraic manipulations) into the standard form of Gauss's hypergeometric equation [20] whereby the acoustic field $\Theta(\theta)$ is obtained as its first series solution that is non-singular at $\theta = 0$ and is given by

$$\Theta(\theta) = P_\nu^{-m} (\cos \theta) = \frac{1}{m!} \left(\frac{1 - \cos \theta}{1 + \cos \theta} \right)^{m/2} {}_2F_1 \left(-\nu; \ \nu + 1; \ 1 + m; \ \frac{1}{2}(1 - \cos \theta) \right), \tag{9}$$

where $P_\nu^{-m}(\cos\theta)$ is the well-known Associated Legendre function of non-integer degree ν and integer order m whilst ${}_2F_1\left(-\nu;\ \nu+1;\ 1+m;\ (1-\cos\theta)/2\right)$ represents the hypergeometric function [20, 21] computed in MATLAB by using the in-built routine $hypergeom\left([a,b],c,y\right)$.

(a)

(b)   **(c)**
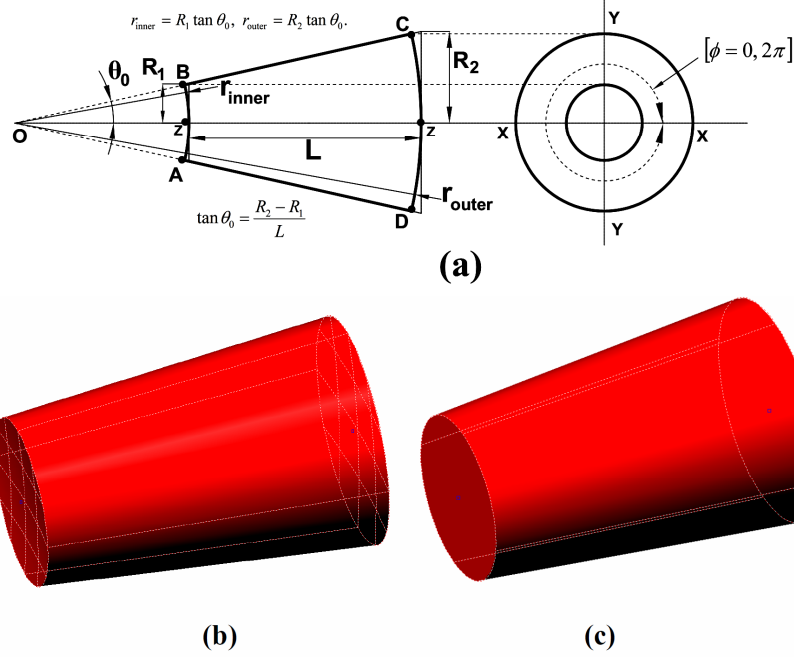
Figure 1. (a) Comparison of the conical chamber with a spherical end face and a flat end face: Front and side view. The 3-D view of a conical chamber with (b) spherical end faces and (c) flat end faces.

The permissible values of non-integer degree ν are computed by substituting $\Theta(\theta)=P_\nu^{-m}(\cos\theta)$ in Eq. (8) following which the 2nd order central Finite Difference (FD) scheme [22] is used to evaluate the first derivative to yield

$$\left.\frac{dP_\nu^{-m}(\cos\theta)}{d\theta}\right|_{\theta=\theta_0}=\frac{P_\nu^{-m}\left(\cos(\theta_0+\Delta\theta_0)\right)-P_\nu^{-m}\left(\cos(\theta_0-\Delta\theta_0)\right)}{2\Delta\theta_0}=0,\ \ \Delta\theta_0=10^{-6}. \tag{10}$$

For a given flare angle θ_0 and azimuthal mode number $m = 0, 1, 2,\dots$, one obtains an infinite sequence of non-integer degree ν values that are numerically computed the Root-Bracketing method [23]. In this paper, a conical chamber having a flare angle $\theta_0 = 5°$ is considered. Table 1 presents the first five non-integer degree values $\nu_n, n=1,\dots,5$ corresponding to the first five azimuthal modes $m = 0$, $1,\dots,4$ for $\theta_0 = 5°$. Henceforth, ν_n^m denotes the non-integer degree in $P_{\nu_n^m}^{-m}(\cos\theta)$ corresponding to the nth zero of Eq. (10) for the azimuthal mode m. The acoustic pressure field $R(r)$ is given by

$$R(r)=A_{1,\nu_n^m}\,j_{\nu_n^m}\left(k_0 r\right)+A_{2,\nu_n^m}\,n_{\nu_n^m}\left(k_0 r\right), \tag{11}$$

where $j_{\nu_n^m}(\cdot)$ and $n_{\nu_n^m}(\cdot)$ denotes the spherical Bessel and Neumann functions, respectively, of non-integer order ν_n^m whilst A_{1,ν_n^m} and A_{2,ν_n^m} denote arbitrary constants. On imposing rigid-wall boundary conditions along the radial direction at the two spherical end faces (see Figs. 1(a) and (b)) and simplifying the resultant determinantal equation (using recurrence relations [17, 20]), one obtains

$$\left\{\nu_n^m j_{\nu_n^m-1}\left(\alpha_{\nu_n^m l}\right)-\left(\nu_n^m+1\right)j_{\nu_n^m+1}\left(\alpha_{\nu_n^m l}\right)\right\}\left\{\nu_n^m n_{\nu_n^m-1}\left(\beta\alpha_{\nu_n^m l}\right)-\left(\nu_n^m+1\right)n_{\nu_n^m+1}\left(\beta\alpha_{\nu_n^m l}\right)\right\}-$$
$$\left\{\nu_n^m n_{\nu_n^m-1}\left(\alpha_{\nu_n^m l}\right)-\left(\nu_n^m+1\right)n_{\nu_n^m+1}\left(\alpha_{\nu_n^m l}\right)\right\}\left\{\nu_n^m j_{\nu_n^m-1}\left(\beta\alpha_{\nu_n^m l}\right)-\left(\nu_n^m+1\right)j_{\nu_n^m+1}\left(\beta\alpha_{\nu_n^m l}\right)\right\}=0,\ \ \forall m=0,\ 1,\ 2,\dots. \tag{12}$$

where $\beta = r_{\mathrm{inner}}/r_{\mathrm{outer}}$. The solution of Eq. (12) yields $\alpha_{v_n^m l} = k_{v_n^m l} r_{\mathrm{outer}}$ which is the non-dimensional resonance frequency of the lth radial/spherical mode corresponding to the non-integer order v_n^m.

Table 1. Non-integer degree values of the Associated Legendre function for first five azimuthal modes $m = 0, 1,\ldots, 4$ and opening angle $\theta_0 = 5°$ corresponding to rigid-wall boundary condition

$\left.\dfrac{\mathrm{d}P_{v_n^m}^{-m}(\cos\theta)}{\mathrm{d}\theta}\right|_{\theta=\theta_0=\pi/36=5°} = 0$	$m = 0$	$m = 1$	$m = 2$	$m = 3$	$m = 4$
v_1	0.0000	20.6155	34.5252	47.6795	60.4841
v_2	43.4110	60.5987	76.3572	91.3658	105.8950
v_3	79.8943	97.3220	113.7487	129.5273	144.8433
v_4	116.0804	133.6431	150.4266	166.6513	182.4505
v_5	152.1791	169.8259	186.8331	203.3520	219.4830

The 3-D acoustic field inside the rigid-wall conical chamber with spherical end faces is therefore, given by

$$p(r,\theta,\phi) = \sum_{m=0,1,2,\ldots}^{m=\infty} \sum_{n=1,2,\ldots}^{n=\infty} \sum_{l=1,2,\ldots}^{l=\infty} \left\{ j_{v_n^m}\left(\alpha_{v_n^m l}\frac{r}{r_{\mathrm{outer}}}\right) - \kappa_{v_n^m l} n_{v_n^m}\left(\alpha_{v_n^m l}\frac{r}{r_{\mathrm{outer}}}\right) \right\} P_{v_n^m}^{-m}(\cos\theta) \left\{ \begin{array}{l} A_{mnl}^1 \cos(m\phi) + \\ A_{mnl}^2 \sin(m\phi) \end{array} \right\}, \quad (13)$$

where A_{mnl}^1 and A_{mnl}^2 denote arbitrary constants and

$$\kappa_{v_n^m l} = \left\{ v_n^m n_{v_n^m-1}\left(\beta\alpha_{v_n^m l}\right) - \left(v_n^m+1\right) n_{v_n^m+1}\left(\beta\alpha_{v_n^m l}\right) \right\} \Big/ \left\{ v_n^m j_{v_n^m-1}\left(\beta\alpha_{v_n^m l}\right) - \left(v_n^m+1\right) j_{v_n^m+1}\left(\beta\alpha_{v_n^m l}\right) \right\}. \quad (14)$$

It is noted that the rigid-wall modes corresponding to $m = 0$, $v_{n=1}^{m=0} = 0$ and $\alpha_{0,l=1,2,\ldots}$ denote purely spherical modes, i.e., only radial wave propagation. The [**T**] matrix based on 1-D spherical wave propagation [6] may be obtained by considering only these modes in the modal solution. It is also noted that since the rigid-wall conditions are *exactly* satisfied along the radial direction at the spherical end faces of the conical chamber (see Fig. 1(b)), the acoustic field can be expressed in terms of a complete basis of orthogonal modal functions given by Eq. (13). On the other hand, for a conical chamber with flat end faces (see Fig. 1(c)), the rigid-wall conditions cannot be exactly satisfied at the flat end faces using the spherical Bessel/Neumann functions; hence, the modal solution given by Eq. (13) is not strictly valid. However, for small flare angle $\theta \leq 5°$, the volume of chambers with flat end faces and spherical end faces are nearly equal and it will be shown later that for such case, there is no appreciable difference in their acoustic attenuation performance.

2.3 Acoustic pressure response expressed in terms of Green's function: Point-source modelling

The acoustic pressure response (modelling the inlet port as a point-source) is obtained in terms of the Green's function solution of the 3-D inhomogeneous Helmholtz equation shown as follows.

$$\frac{p(r_R,\theta_R,\phi_R|r_S,\theta_S,\phi_S)}{\rho_0 Q_0} = \frac{G(r_R,\theta_R,\phi_R|r_S,\theta_S,\phi_S)}{\rho_0 Q_0} =$$

$$jk_0 c_0 \sum_{m=0,1,2,\ldots}^{\infty} \sum_{l=0,1,2,\ldots}^{\infty} \sum_{n=0,1,2,\ldots}^{\infty} \left\{ \begin{array}{l} \dfrac{\left\{R(r=r_S)P_{v_n^m}^{-m}(\cos\theta_S)\cos(m\phi_S)\right\} \times \left\{R(r=r_R)P_{v_n^m}^{-m}(\cos\theta_R)\cos(m\phi_R)\right\}}{\left(k_{v_n^m l}^2 - k_0^2\right) N_{v_n^m, l, m}} + \\[2em] \dfrac{\left\{R(r=r_S)P_{v_n^m}^{-m}(\cos\theta_S)\sin(m\phi_S)\right\} \times \left\{R(r=r_R)P_{v_n^m}^{-m}(\cos\theta_R)\sin(m\phi_R)\right\}}{\left(k_{v_n^m l}^2 - k_0^2\right) N_{v_n^m, l, m}} \end{array} \right\}, \quad (15)$$

where Q_0 is the volume flow-rate $\left(\mathrm{m}^3\cdot\mathrm{s}^{-1}\right)$ due to point-source port, $\left(r_S,\theta_S,\phi_S\right)$ and $\left(r_R,\theta_R,\phi_R\right)$ are the co-ordinates of the centre of the source and receiver ports, respectively, whilst

$$R(r)=\left\{j_{v_n^m}\left(\alpha_{v_n^m l}\frac{r}{r_{\mathrm{outer}}}\right)-\kappa_{v_n^m l}n_{v_n^m}\left(\alpha_{v_n^m l}\frac{r}{r_{\mathrm{outer}}}\right)\right\},\quad k_{v_n^m l}=\alpha_{v_n^m l}/r_{\mathrm{outer}}\,,\tag{16}$$

and $N_{v_n^m,l,m}$ denotes the integrals of the square of the product of a particular set of orthogonal modal functions defined over the conical chamber volume and evaluated analytically [24].

2.4 Acoustic pressure response based on the uniform piston-driven model

The mathematically more accurate *uniform piston-driven* model [18, 25, 26] is now used to obtain the [**Z**] matrix parameters for different configurations of the source and receiver ports shown as follows.

(a) *Source and receiver ports both located on spherical end faces*

$$Z_{E2E1}=\frac{R_{E2}^2}{S_{E2}}\iint_{S_{E2}}\left\{\frac{R_{E1}^2}{S_{E1}}\iint_{S_{E1}}\frac{G\left(r_{E2}=R_{E2},\theta_{E2},\phi_{E2}\middle|r_{E1}=R_{E1},\theta_{E1},\phi_{E1}\right)}{\rho_0 Q_0}\sin\theta_{E1}d\theta_{E1}d\phi_{E1}\right\}\sin\theta_{E2}d\theta_{E2}d\phi_{E2}.\tag{17}$$

(b) *Source port located on a spherical end face and receiver port located on the side surface*

$$Z_{S1E1}=\frac{\sin\theta_0}{S_{S1}}\iint_{S_{S1}}\left\{\frac{R_{E1}^2}{S_{E1}}\iint_{S_{E1}}\frac{G\left(r_{S1},\theta_{S1}=\theta_0,\phi_{S1}\middle|r_{E1}=R_{E1},\theta_{E1},\phi_{E1}\right)}{\rho_0 Q_0}\sin\theta_{E1}d\theta_{E1}d\phi_{E1}\right\}r_{S1}dr_{S1}d\phi_{S1}.\tag{18}$$

(c) *Source and receiver ports both located on the side surface*

$$Z_{S2S1}=\frac{\sin\theta_0}{S_{S2}}\iint_{S_{S2}}\left\{\frac{\sin\theta_0}{S_{S1}}\iint_{S_{S1}}\frac{G\left(r_{S2},\theta_{S2},\phi_{S2}\middle|r_{S1},\theta_{S1},\phi_{S1}\right)}{\rho_0 Q_0}r_{S1}dr_{S1}d\phi_{S1}\right\}r_{S2}dr_{S2}d\phi_{S2}.\tag{19}$$

The mathematical forms of the integral of the Green's function over the end or side port in Eqs. (17-19) as well as the effect of port location on the propagation/suppression of certain modes on the [**Z**] matrix parameters are discussed in a greater detail in Ref. [24].

2.5 Computation of TL performance in terms of [Z] matrix parameters

An expression for TL performance of a SISO system is obtained in terms of the $\left[\mathbf{Z}\right]$ matrix parameters. To this end, the relation between the scattering $\left[\mathbf{S}\right]$ matrix and the $\left[\mathbf{Z}\right]$ matrix is first presented [15].

$$\left\{\begin{matrix}B_1\\B_2\end{matrix}\right\}=\left[\mathbf{S}\right]\left\{\begin{matrix}A_1\\A_2\end{matrix}\right\},\quad\left[\mathbf{S}\right]_{2\times2}=\begin{bmatrix}S_{11}&S_{12}\\S_{21}&S_{22}\end{bmatrix},\quad\left[\mathbf{S}\right]=\mathbf{I}-2\left[\left[\mathbf{Z}\right]\begin{bmatrix}1/Y_1&0\\0&1/Y_2\end{bmatrix}+\mathbf{I}\right]^{-1},\tag{20-22}$$

where $\{B_1,B_2\}$ and $\{A_1,A_2\}$ are the incident and reflected progressive-wave amplitudes, respectively, at the ports, $\mathbf{I}$ is the identity matrix whilst Y_1 and Y_2 are the characteristic impedances at ports 1 and 2, respectively. A uniform piston excitation is applied at the port 1 (inlet) whilst anechoic termination is imposed at the port 2 (outlet), thereby implying $A_2=0$. The TL is therefore, given by [15, 18, 25]

$$\mathrm{TL}=10\log_{10}\left(\frac{Y_2}{Y_1}\frac{1}{|S_{21}|^2}\right)=10\log_{10}\left(\frac{1}{4Y_1Y_2}\left|\frac{\left(Z_{11}+Y_1\right)\left(Z_{22}+Y_2\right)-Z_{21}Z_{12}}{Z_{21}}\right|^2\right).\tag{23}$$

3. Results, Analysis and Formulation of Design Guidelines

Figures 2(a-e) show the three orthogonal views of different configurations of the 2-port SISO conical mufflers having ports located either on the spherical end faces or the side (curved) surface. These configurations are briefly described in a sequential manner as follows.
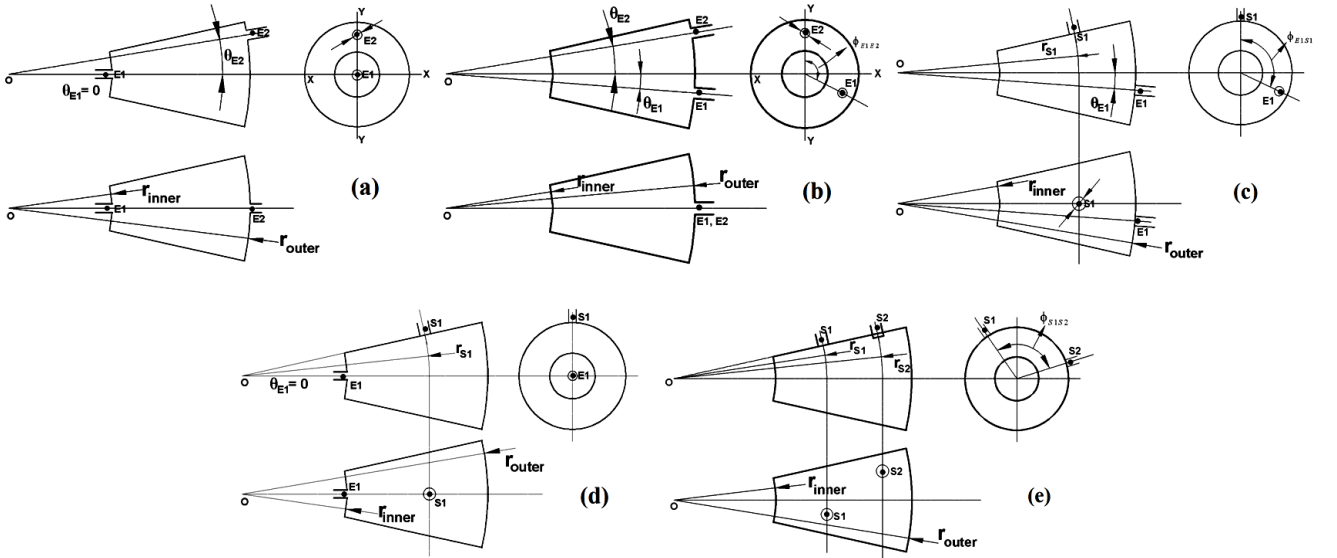
Figure 2. A 2-port (SISO) conical chamber muffler having (a) an end-centred port E1 and end-offset port E2 located on the inner and outer spherical end faces, respectively, (b) end-offset ports E1 and E2 located on the same (outer) spherical end face, (c) an end-offset port E1 located on the outer spherical end face and side port S1, (d) an end-offset port E1 located on the inner spherical end face and side port S1 and (e) two side ports S1 and S2.

Figure 2(a) shows a conical expansion chamber having an end-centred port (denoted by E1) and end-offset port (denoted by E2) located on the inner and outer spherical end faces, respectively. Such a configuration is referred to as a *straight-flow* configuration. It is noted that an end-centred port E1 implies that its polar angular location $\theta_{E1} = 0$, i.e., the end-port is concentric with the inner spherical end face whilst the angular location of end port E2 is denoted by θ_{E2}. Figure 2(b) shows a conical chamber having end-offset inlet port E1 and end-offset outlet port E2, both located on the outer spherical end face. The polar angular location of the end ports is denoted by θ_{E1} and θ_{E2}, respectively, whilst their relative azimuthal angular location is denoted by ϕ_{E1E2}. Such a configuration is referred to as a *flow-reversal* configuration. Figures 2(c) and (d) show a conical chamber having a side port S1 and an end port E1 located on the outer and inner spherical end faces, respectively. While an end-centred port E1 is considered in Fig. 2(d), the polar angular location of the end-offset port E1 in Fig. 2(c) is taken in general, as θ_{E1} whilst the relative azimuthal angle is denoted by ϕ_{E1S1}. Figure 2(e) shows a conical chamber having two side ports S1 and S2 located at radial distance r_{S1} and r_{S2}, respectively, whilst their relative azimuthal angular location is denoted by ϕ_{S1S2}. Configurations (c-e) are referred to as *cross-flow* configuration.

The cross-sectional radius R_1 of the inner spherical end face is taken equal to $75\,\text{mm}$ and for flare angle $\theta = 5°$, one obtains $r_{\text{inner}} = 857.25$ mm. A radially long conical chamber of length $L = 300$ mm is considered in this work which implies $r_{\text{outer}} = 1157.25$ mm. The cross-sectional radius R_2 of the outer spherical end face is therefore, equal to 101.25 mm. Furthermore, the port diameters are considered equal and taken as 40 mm whilst the sound speed $c_0 = 343.14$ m·s^{-1}. It is noted that only the first five azimuthal modes, i.e., $m = 0, 1, …, 4$, the first five non-integer degree values corresponding to each azimuthal order m, i.e., $v_n^m, n = 1, 2, …, 5$ and the first eight radial modes corresponding to each non-integer degree value and azimuthal order m, i.e., $\alpha_{v_n^m l}$, $m = 0…4$, $n = 1…5$, $l = 1…8$ are considered in the Green's function given by Eq. (15). The truncation of the modal solution to these first few modes ensures a good convergence of the acoustic pressure response due to the uniform piston-driven model.

3.1 End-inlet and end-outlet muffler

Figure 3(a) compares the TL performance of concentric conical muffler shown in Fig. 2(a) wherein

$\theta_{E1} = \theta_{E2} = 0$ obtained using the 3-D semi-analytical formulation with 3-D FEA prediction.
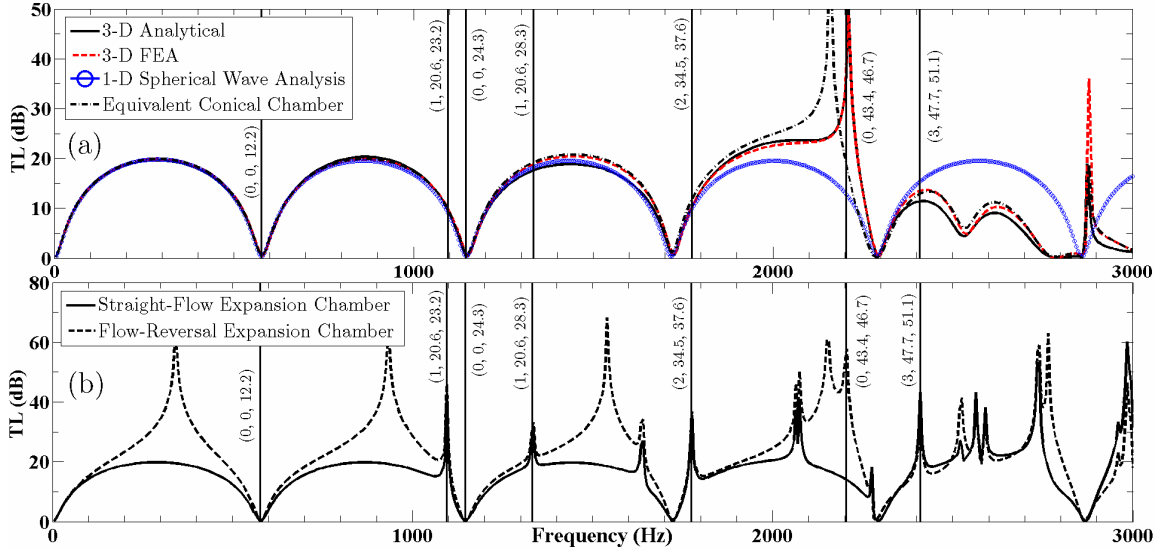
Figure 3. (a) Comparison of the TL performance of the conical muffler configuration shown in Fig. 2(a) with the following port location: r_{E1} = 857.25 mm, r_{E2} = 1157.25 mm and $\theta_{E1} = \theta_{E2} = 0$ obtained using the 3-D semi-analytical, 3-D FEA and 1-D spherical wave analysis, (b) TL performance of the conical muffler configurations shown in Figs. 2(a) and (b) with polar angular location of the end-inlet and end-outlet ports taken as $\theta_{E1} = 0$ and $\theta_{E2} = 3.14°$.

It is observed from Fig. 3(a) that both analytical and numerical 3-D approaches are in excellent agreement throughout the frequency range of interest, thereby validating the semi-analytical approach. It is noted that vertical lines in Fig. 2(a) denotes the resonance frequency of $\left(m, v_n^m, \alpha_{v_n^m l} \right)$ mode of the conical muffler and the same convention is followed in the remaining TL graphs. The TL graph resembles that of a concentric expansion chamber having a uniform cross-section area [6, 27]; it exhibits a pattern of frequency attenuation domes followed by troughs at the resonance frequency of purely spherical/radial modes. This pattern breaks down at the onset of (0, 43.4, 46.7) circumferential mode. The 1-D spherical wave analysis [6] is in a good agreement with 3-D approaches up to the resonance frequency of the third spherical mode beyond which the 1-D analysis fails as significant deviations are observed. Furthermore, an excellent agreement of TL graph of conical chamber having flat end faces (computed using 3-D FEA) with chambers having spherical end faces suggests that the 3-D modal solution given by Eq. (15) can also be used for accurately evaluating the TL performance of chambers with flat end faces, at least for small flare angles.

Figure 3(b) shows the TL performance for conical muffler configurations shown in Figs. 2(a) and (b) wherein $\theta_{E1} = 0$ and $\theta_{E2} = 3.14°$ for both cases. It is observed that the TL graph for straight-flow configuration in Fig. 3(b) resembles that shown in Fig. 3(a) for the concentric conical chamber case; however, due to the offset location of end-port E2 in this case, azimuthal modes are also excited which influence the attenuation performance as evidenced from the existence of peaks at their respective resonance frequencies. On the other hand, the TL graph for the flow-reversal configuration shown in Fig. 3(b) exhibits a pattern of attenuation peaks followed by troughs that resemble the TL characteristics of axially long flow-reversal circular/elliptical cylindrical chamber [28, 29].

3.2 End-inlet and side-outlet muffler

Figure 4(a) compares the TL performance of conical muffler configuration shown in Fig. 2(d) having end-centred inlet port E1 and a side outlet port S1 located at r_{S1} = 1016.32 mm obtained using the 3-D semi-analytical method with 3-D FEA prediction. An excellent agreement between both analytical and numerical 3-D approaches throughout the frequency range of interest, demonstrates the accuracy of the semi-analytical approach for the end-inlet and side-outlet configuration. A broadband attenuation performance is observed up to resonance frequency of the (0, 0, 24.3) spherical mode which is

8

explained on the basis of radial location of ports. The radial location r_{S1} of side port S1 on the pressure node of the (0, 0, 12.2) mode and the location of end port E1 on the inner spherical end face nullifies the trough at the resonance frequency of this modes resulting in attenuation peak. Therefore, by suppressing the first radial mode at its resonance frequency, a broadband TL performance is obtained. In fact, the TL performance of the end-inlet and side-outlet conical muffler is qualitatively similar to that of an end-inlet and side-outlet muffler having a uniform cross-sectional area [25, 30].
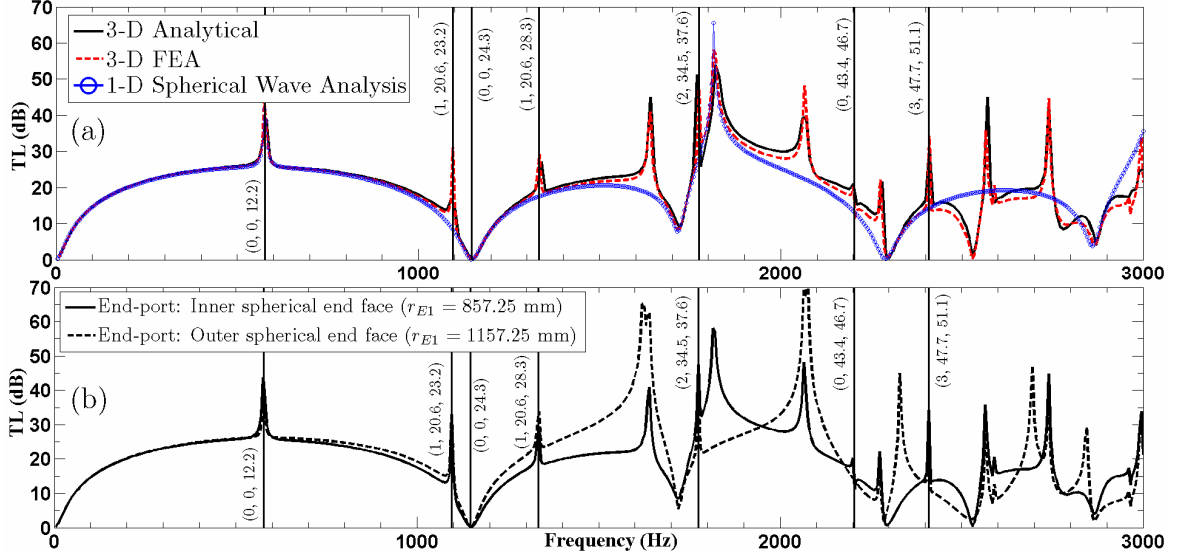
Figure 4. (a) Comparison of the TL performance of the conical muffler configuration shown in Fig. 2(d) having the following port location: r_{E1} = 857.25 mm, r_{S1} = 1016.32 mm and $\theta_{E1} = 0$ obtained using the 3-D semi-analytical, 3-D FEA and 1-D spherical wave analysis. (b) TL performance of the muffler configurations shown in Figs. 2(c) and (d) both having a concentric end port E1, i.e., $\theta_{E1} = 0$ whilst the radial location of the side port S1 is identical with that considered in part (a).

Figure 4(b) investigates the effect of changing the location of end port E1 from the inner spherical end face to the outer spherical end face whilst keeping the radial location of the side port constant. It is observed from Fig. 4(b) that there is no appreciable difference in the TL graphs when $r_{E1} = 857.25$ mm and $r_{E1} = 1157.25$ mm, at least in the low-frequency range up to the resonance frequency of the (1, 20.6, 28.3) azimuthal mode beyond which significant deviations are noticeable. In fact, the configuration with $r_{E1} = 1157.25$ mm exhibits slightly improved TL performance.

3.3 Side-inlet and side-outlet muffler

Figure 5(a) compares the TL performance of conical muffler configuration shown in Fig. 2(e) having $\phi_{S1S2} = \pi/2$, r_{S1} = 1016.32 mm and r_{S2} = 1084.39 mm obtained using the 3-D semi-analytical method with 3-D FEA prediction. An excellent agreement between both analytical and numerical 3-D approaches throughout the frequency range of interest, confirms the accuracy of the semi-analytical approach for the side-inlet and side-outlet configuration. A broadband attenuation performance is observed from Fig. 5(a) up to resonance frequency of the (2, 34.5, 37.6) azimuthal mode which is explained on the basis of radial and relative azimuthal angular location of side ports. The radial location r_{S1} of side port S1 on the pressure node of the (0, 0, 12.2) mode and the radial location r_{S2} of side port S2 on *one* of the pressure nodes of the (0, 0, 24.3) mode nullifies the trough at the resonance frequency of these modes resulting in attenuation peak. Furthermore, the relative polar angular location $\phi_{S1S2} = \pi/2$ nullifies the trough at the resonance frequency of the (1, 20.6, 23.2) and (1, 20.6, 28.3) azimuthal modes yielding attenuation peak. In view of suppression of the first few radial and azimuthal modes at their respective resonance frequencies, one obtains broadband TL characteristics. In fact, the TL performance of the side-inlet and side-outlet conical muffler is qualitatively similar to that of a side-inlet and side-outlet muffler having a uniform cross-sectional area [26, 30].
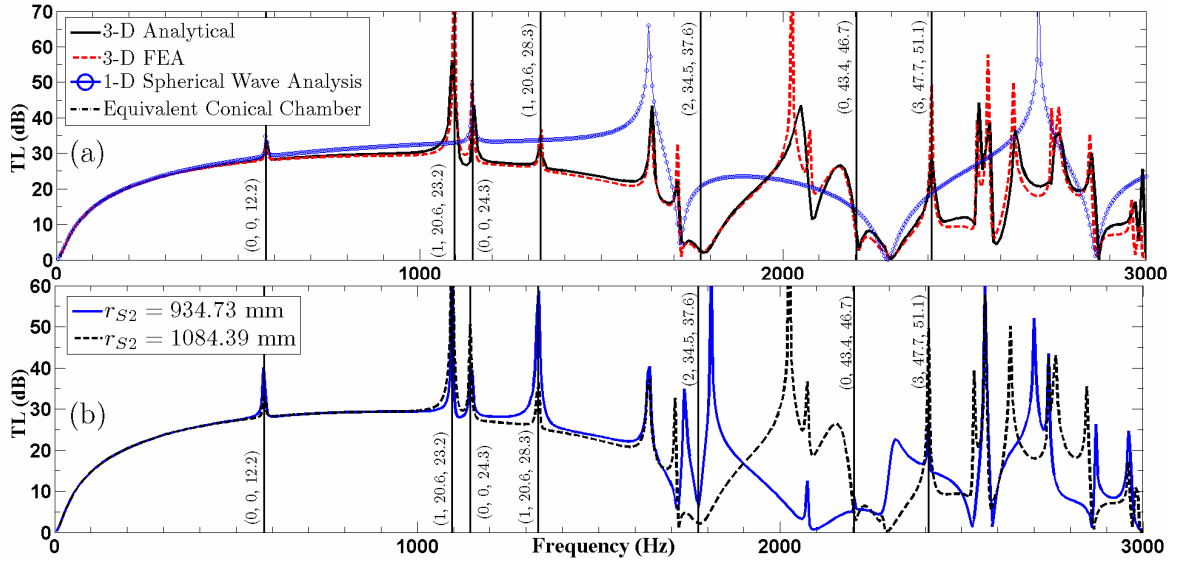
Figure 5. (a) Comparison of the TL performance of the muffler configuration shown in Fig. 2(e) having the following port location: r_{S1} = 1016.32 mm, r_{S2} = 1084.39 mm and $\phi_{S1S2} = \pi/2$ obtained using the 3-D semi-analytical, 3-D FEA and 1-D spherical wave analysis. (b) Effect of change in location of the side port S2 from the radial nodes r_{S2} = 1084.39 mm to r_{S2} = 934.73 mm both corresponding to (0, 0, 24.3) spherical mode.

It is observed from Fig. 5(a) that the TL obtained using the 1-D spherical wave analysis [6] matches well with the 3-D approaches up to the resonance frequency of the second spherical mode beyond which the 1-D analysis is not valid as significant deviations are observed. Furthermore, a complete overlap of the TL graphs of conical chamber having flat end faces and that with spherical end faces again demonstrates that 3-D modal solution given by Eq. (15) can also be used for accurately evaluating the TL performance of chambers with flat end faces, at least for small flare angles.

Figure 5(b) investigates the effect of varying the radial location of side port S2 from radial nodes r_{S2} = 1084.39 mm to r_{S2} = 934.73 mm both corresponding to (0, 0, 24.3) spherical mode whilst keeping the radial location r_{S1} = 1016.32 mm of the side port S1 constant. It is observed that there are no significant differences between the TL performance of the two configurations up to the resonance frequency of the (2, 34.5, 37.6) azimuthal mode beyond which the deviations are inconsequential insofar as design criteria is considered.

4. Conclusions

This paper has analysed the Transmission Loss (TL) performance of a SISO conical muffler by means of a 3-D semi-analytical uniform piston-driven model based on the modal expansion technique and the Green's function approach. The 3-D modal expansion includes the azimuthal or non-axisymmetric modes (for which $m \neq 0$, $n = 1, 2,..., l = 1, 2,...$) in addition to the inclusion of the purely spherical modes (which depends only on the radial co-ordinates wherein $v_{n=1}^{m=0} = 0$, $m = 0$, $n = 1$, $l = 1, 2,...$) and the axisymmetric or circumferential modes (which depends on the polar angular and radial co-ordinates wherein $v_{n \neq 1}^{m=0} \neq 0$, $m = 0$, $n \neq 1$, $l = 1, 2,...$). This enables one to analyse conical muffler configurations having arbitrary location of ports on chamber surface such as an end-offset port or a side port. The TL performance predicted by the 3-D semi-analytical approach is in an excellent agreement with 3-D FEA predictions, thereby validating the approach presented here.

A parametric investigation (based on the 3-D semi-analytical approach) on the effect of location of ports was conducted resulting in the formulation of guidelines in terms of optimal port location for designing SISO conical mufflers exhibiting a broadband TL performance that are indicated as follows. (a) *Radially long* configuration having a side-inlet port S1 located on the pressure node of the first spherical/radial mode, i.e., $(0, 0, \alpha_{v_{n=1}^{m=0}l=1})$ mode and a side-outlet port S2 located on one of the pressure nodes of the second spherical/radial mode, i.e., $(0, 0, \alpha_{v_{n=1}^{m=0}l=2})$ mode with relative azimuthal

angular location of the side ports given by $\phi_{S1S2} = \pi/2$.

(b) *Radially long* configuration having a side-inlet/outlet port S1 located on the pressure node of the first radial mode and a *concentric* end-outlet/inlet port E1 located on the inner/outer spherical end face.

(c) *Radially long* configuration having a side-inlet/outlet port S1 located on the pressure node of the first radial mode and an end-offset outlet/inlet port E1 located on the inner/outer spherical end face with its centre coincident with pressure nodal angle of the $P_{v^{m=0}_{n=2}}^{m=0}(\cos\theta)$ mode whilst the relative azimuthal angular location of the end and side ports given by $\phi_{E1S1} = \pi/2$.

Acknowledgement

References

[1]   Rayleigh, L. *The Theory of Sound*, Vol. 1 and 2, Dover publications, New York, 1896.
[2]   Webster, A. G. "Acoustical impedance, and the theory of horns and of the phonograph", *Journal of National Academy of Sciences*, **5**, 275-282, (1919).
[3]   Mawardi, O. K. "Generalized solutions of Webster's horn theory", *Journal of Acoustical Society of America*, **21**, 323-330, (1949).
[4]   Davies, P. O. A. L. and Doak, P. E. "Spherical wave propagation in conical pipe with mean flow", *Journal of Sound and Vibration*, **137**, 343-346, (1990).
[5]   Miles, J. H. "Acoustic transmission of a variable area duct or a nozzle carrying compressible subsonic flow", *Journal of Acoustical Society of America*, **69**, 1577-1586 (1981).
[6]   Munjal, M. L. *Acoustics of Ducts and Mufflers*, Wiley, Chichester, 2014.
[7]   Easwaran, V. and Munjal, M. L. "Plane wave analysis of conical and exponential pipes with incompressible mean flow", *Journal of Sound and Vibration,* **152**, 73-93 (1992).
[8]   Gupta, V. H., V. Easwaran, V. and Munjal, M. L. "A modified segmentation approach for analyzing plane wave propagation in non-uniform ducts with mean flow", *Journal of Sound and Vibration*, **182**, 697-707, (1995).
[9]   Astley, R. J. and Eversman, W. "A Finite element method for transmission in non-uniform ducts without flow: Comparison with the method of weighted residuals", *Journal of Sound and Vibration,* **57**, 367-388, (1978).
[10]   Astley, R. J. and Eversman, W. "Acoustic transmission in non-uniform ducts with mean flow. Part II: The finite element method", *Journal of Sound and Vibration*, **74**, 103-121, (1981).
[11]   Alfredson, R. J. "The propagation of sound in a circular duct of continuously varying cross-sectional area", *Journal of Sound Vibration,* **23**, 433-442, (1972).
[12]   Cummings, A. "Acoustics of a wine bottle", *Journal of Sound Vibration,* **31**, 331-343 (1973).
[13]   Willatzen, M. "The influence of a liquid flow on sound fields confined by conical walls", *Journal of Sound Vibration*, **248**, 847-863, (2001).
[14]   Denia, F. D., Fuenmayor, F. J. and Carballeira, J. "Three-dimensional analysis of mufflers with conical ducts: Analytical, numerical and experimental studies", 32nd *International Congress and Exposition on Noise Control Engineering, Proceedings of Internoise* 2003, Seogwipo, Korea, 25-28 August 2003.
[15]   Mimani, A. and Munjal, M. L. "Acoustical analysis of a general network of multi-port elements - An impedance matrix approach", *International Journal of Acoustics and Vibration*, **17**, 23-46, (2012).
[16]   Easwaran, V., Gupta, V. H. and Munjal, M. L. "Relationship between the impedance matrix and the transfer matrix with specific reference to symmetrical, reciprocal and conservative systems", *Journal of Sound and Vibration*, **161**, 515-525, (1993).
[17]   Blackstock, D. T. *Fundamentals of Physical Acoustics*, Wiley, New York, 2000.
[18]   Mimani, A. and Munjal, M. L. "3-D acoustic analysis of spherical chamber having single inlet and multiple outlet: An impedance matrix approach", *International Journal of Applied Mechanics*, **3**, 685-710, (2011).

[19] Mimani, A. "Broadband transmission loss performance of a hemispherical end-chamber muffler with single end-inlet and single/double end-outlet", *Proceedings of Acoustics 2015*, Hunter Valley, NSW, Australia, 15-18 November 2015.

[20] Arfken, G. B. and Weber, H. J. *Mathematical Methods for Physicists*, Academic Press, Elsevier, London, 2005.

[21] Olver, F. W. J. and Smith, J. M. "Associated legendre functions on the cut", *Journal of Computational Physics*, **51**, 502-518, (1983).

[22] Tam, C. K. W. *Computational aeroacoustics – A wave number approach*, Cambridge University Press, New York, 2012.

[23] Kreyszig, E. *Advanced Engineering Mathematics*, Wiley, New-Delhi, 1999.

[24] Mimani, A. "1-D and 3-D analysis of multi-port muffler configurations with emphasis on elliptical cylindrical chamber", *Ph. D. Thesis*, Indian Institute of Science, Bangalore, March 2012.

[25] Mimani, A. and Munjal, M. L. "3-D acoustic analysis of elliptical chamber mufflers having an end-inlet and a side-outlet: An impedance matrix approach", *Wave Motion*, **49**, 271-295, (2012).

[26] Mimani, A. and Munjal, M. L. "Acoustical behavior of single inlet and multiple outlet elliptical cylindrical chamber muffler", *Noise Control Engineering Journal*, **60**, 605-626, (2012).

[27] Selamet, A. and Radavich, P. M. "The effect of length on acoustic attenuation performance of concentric expansion chambers: An analytical, computational and experimental investigation", *Journal of Sound and Vibration*, **201**, 407-426, (1997).

[28] Mimani, A. and Munjal, M. L. "On the role of higher-order evanescent modes in end-offset inlet and end-centered outlet elliptical flow-reversal chamber mufflers", *International Journal of Acoustics and Vibration*, **17**, 139-154, (2012).

[29] Mimani, A. and Munjal, M. L. "Acoustic end-correction in a flow-reversal end chamber muffler: A semi-analytical approach", Accepted for publication in the *Journal of Computational Acoustics* on the 1st October, 2015.

[30] Munjal, M. L. "Plane wave analysis of side inlet/outlet chamber mufflers with mean flow", *Applied Acoustics*, **52**, 165-175, (1997).